



**HAL**  
open science

## Investigations of the Co-Pt alloy phase diagram with neutron diffuse scattering, inverse cluster variation method and Monte Carlo simulations

Mathieu Fèvre, Juan M. Sanchez, Ross J.R. Stewart, Jean Sébastien Mérot, Frédéric Fossard, Yann Le Bouar, Katsushi Tanaka, Hiroshi Numakura, Guy Schmerber, Véronique Pierron-Bohnes

### ► To cite this version:

Mathieu Fèvre, Juan M. Sanchez, Ross J.R. Stewart, Jean Sébastien Mérot, Frédéric Fossard, et al.. Investigations of the Co-Pt alloy phase diagram with neutron diffuse scattering, inverse cluster variation method and Monte Carlo simulations. *Physical Review B*, 2020, 102 (13), 10.1103/PhysRevB.102.134114 . hal-02979606

**HAL Id: hal-02979606**

**<https://hal.science/hal-02979606>**

Submitted on 27 Oct 2020

**HAL** is a multi-disciplinary open access archive for the deposit and dissemination of scientific research documents, whether they are published or not. The documents may come from teaching and research institutions in France or abroad, or from public or private research centers.

L'archive ouverte pluridisciplinaire **HAL**, est destinée au dépôt et à la diffusion de documents scientifiques de niveau recherche, publiés ou non, émanant des établissements d'enseignement et de recherche français ou étrangers, des laboratoires publics ou privés.

# Investigations of the Co-Pt alloy phase diagram with neutron diffuse scattering, inverse cluster variation method and Monte Carlo simulations

M. Fèvre<sup>1,\*</sup>, J.-M. Sanchez<sup>2</sup>, J. R. Stewart<sup>3</sup>, J.-S. Mérot<sup>1</sup>, F. Fossard<sup>1</sup>, Y. Le Bouar<sup>1</sup>, K. Tanaka<sup>4</sup>, H. Numakura<sup>5</sup>, G. Schmerber<sup>6</sup>, and V. Pierron-Bohnes<sup>6</sup>

<sup>1</sup> *Université Paris-Saclay, ONERA, CNRS,*

*Laboratoire d'étude des microstructures, 92322, Châtillon, France*

<sup>2</sup> *The American University of Sharjah,*

*University City, PO Box 26666, Sharjah, UAE*

<sup>3</sup> *ISIS Facility, Rutherford Appleton Laboratory,*

*Harwell Campus, Didcot OX11 0QX, UK*

<sup>4</sup> *Department of Mechanical Engineering, Kobe University,*

*1-1 Rokkoudai-cho, Nada-ku, Kobe 657-8501, Japan*

<sup>5</sup> *Department of Materials Science,*

*Osaka Prefecture University, Gakuencho 1-1,*

*Naka-ku, Sakai 599-8531, Japan and*

<sup>6</sup> *Université de Strasbourg, CNRS,*

*Institut de Physique et Chimie des Matériaux de Strasbourg,*

*UMR 7504, 23 rue du Loess BP 43,*

*F-67034 Strasbourg, France*

(Dated: September 21, 2020)

## Abstract

The short-range order in a CoPt alloy was determined at 1203 K and 1423 K using neutron diffuse scattering measurements. The effective pair interactions provided by data analysis reproduce well the experimental order-disorder transition temperature in Monte Carlo simulations. They complete previous results reported for the Co-Pt system and are compared to those obtained within tight-binding and *ab initio* formalisms. Our results show that the important dependence of the nearest-neighbor pair interactions with composition is not related to the sample magnetic state at the measured temperatures. Interactions measured in the paramagnetic domain for the CoPt alloy behave like those in the ferromagnetic domain for the Co<sub>3</sub>Pt and Co<sub>0.65</sub>Pt<sub>0.35</sub> alloys. The effective pair interactions related to the tight-binding Ising model provide a relatively good description of the CoPt alloy thermodynamics close to the ordering temperature (short-range order and temperature of phase transformation), even if they strongly differ from those measured in this study. The average magnetic moment of Co atoms at high temperatures was determined from the analysis of the intensity contribution that is not dependent on the scattering vector. The obtained value is very close to the moment measured at room temperature or determined from *ab initio* calculations. This confirms the Curie-Weiss behavior of the CoPt alloy. Finally, transmission electron microscope observations carried out on samples annealed for about 30 days confirmed that the order-disorder transition takes place in the 830 K-843 K temperature interval at the Co<sub>3</sub>Pt composition.

PACS numbers: 61.12.Ex, 64.60.De, 64.60.Cn, 75.50.Cc,81.30.Bx

## I. INTRODUCTION

Understanding the mechanisms governing the phase stability of alloys is essential to predict the modification of their bulk physical properties by surface or confined effects. This has important consequences especially in catalysis, optic, plasmonic or magnetic based applications. In all generality, in metals, transformation temperatures can be sustained by different effects such as chemical, elastic, electronic or magnetic interactions and couplings. Identifying the major contributions which must be incorporated in models to reproduce the thermodynamics of alloys is therefore important. For the Co-Pt system, this task has not been fully completed yet. At the present time, an accurate description of the concentration-temperature phase diagram of the Co-Pt system by atomistic approaches is still absent.

In the solid state,  $\text{Co}_{1-x}\text{Pt}_x$  alloys exhibit three ordered phases with the classical AuCu ( $L1_0$ ) and  $\text{AuCu}_3$  ( $L1_2$ ) ordered structures around the CoPt,  $\text{CoPt}_3$  and  $\text{Co}_3\text{Pt}$  compositions. Order-disorder transitions take place at temperatures close to 1100 K, 1000 K, and 830 K respectively<sup>1-3</sup>. The difference of 170 K between the ordering temperatures of the  $\text{Co}_3\text{Pt}$  and the  $\text{CoPt}_3$  phases cannot be explained by lattice mismatch ( $\simeq 10\%$ ) and elastic moduli differences ( $\simeq 20\%$ ) between  $\alpha$ -cobalt and platinum. It was suggested by Monte Carlo simulation that in binary A-B alloys of the face centered cubic (FCC) structure the order-disorder transition temperature of  $\text{AB}_3$  is higher than that of  $\text{A}_3\text{B}$  when the atom species B is smaller in size<sup>4</sup>. However, the trend is the opposite in the Co-Pt system<sup>1,5</sup>.

In this system, the Curie temperature decreases rapidly<sup>6</sup> from  $T_{CM} = 1400$  K at  $x = 0$  to  $T_{CM} = 0$  K at  $x = 1.0$ . The ordering transition occurs in the ferromagnetic domain for the  $\text{Co}_3\text{Pt}$  phase and in the paramagnetic domain for the CoPt and  $\text{CoPt}_3$  phases. The importance of magnetism in the formation energies of Co-Pt has been demonstrated using *ab initio* electronic structure calculations<sup>7,8</sup>.

Phase stability and thermodynamics of substitutional binary alloys have been extensively studied on rigid lattices using phenomenological approaches such as lattice gas models coupled to statistical mechanics methods. This consists in describing the internal energy of the alloy by occupational degrees of freedom, related to chemical species, interacting through an Ising-like Hamiltonian which is expressed as a sum of pair and higher order multiplet interactions (triplets, quadruplets, ...). In the general perturbation method, the ordering energy is written as a perturbation development with respect to a reference state corre-

sponding to the random alloy. For phase diagram calculations in transition metal alloys with ordering on a fcc lattice, it has been shown using tight-binding calculations that (i) the pair approximation is valid provided their concentration dependence is taken into account<sup>9,10</sup>, (ii) the magnitude of the effective pair interaction (EPI) follow the hierarchy  $|\tilde{V}_1| \gg |\tilde{V}_2, \tilde{V}_3, \tilde{V}_4| \gg |\tilde{V}_5, \tilde{V}_6, \dots|$ , where  $\tilde{V}_i$  is the EPI related to  $i^{th}$  nearest neighbor sites. A useful consequence of describing binary alloys in terms of EPI rely on the fact that, providing that chemical effects can be separated from other contributions (elastic, magnetic, ...), they can be determined quite simply using diffuse X-ray or neutrons scattering experiments. The pair interaction approximation therefore provides a framework where outcomes arising from experiments and first principles calculations can be confronted or combined. However, due to its simplicity, this approach suffers from several general limitations : (i) the described model is relevant when chemical effects are the driving force of the phase stability. For the L1<sub>0</sub>-A1 transition, this condition is fulfilled since the primary order parameter is related to chemical ordering whereas the deformation of the unit cell is a secondary order parameter<sup>11</sup>, (ii) EPI are determined for a given alloy composition. The formalism is in principle not relevant if the phase transition involves two-phase domains where the concentrations related to the coexisting phases significantly differ from the concentration corresponding to the disordered state.

At the CoPt composition, the derivation of EPI from the formation energy of stable and metastable phases led to a transition temperature which was about half of the measured one<sup>12</sup>. This suggests that some effects not taken into account in the *ab initio* calculations and in the cluster expansion (CE) formalism<sup>13</sup> prevent the accurate prediction of the transition temperature. This could be the contributions of the vibrational free energy<sup>14</sup> or electronic excitations<sup>15</sup>.

The short- and long-range orders (SRO and LRO) developing in the disordered state close to solid-solid phase transitions have been investigated using neutron and X-ray diffuse scattering experiments near the Co<sub>3</sub>Pt and CoPt<sub>3</sub> compositions<sup>5,16</sup>. The EPI calculated with the Inverse Cluster Variation Method<sup>17</sup> (ICVM) exhibit an important composition dependence of the nearest neighbor pair interaction energy. As the measurements on Co<sub>3</sub>Pt were carried out in the ferromagnetic domain whereas those on CoPt<sub>3</sub> were made in the paramagnetic domain, this behavior could be attributed to the effect of magnetism. Similar measurements at the CoPt composition could answer this question. The Monte Carlo simulations performed

on a rigid face centered cubic (FCC) lattice with the derived EPI succeeded in reproducing the experimental ordering temperatures. This shows that effective pair interactions determined from diffuse scattering measurements on Co-Pt alloys can be used as quantitative data for developing atomic interaction potentials – implemented on- or off-lattices – capable of describing accurately the main features of the alloy phase diagram (ordering temperatures, asymmetry, compositions related to congruent transformations). This step is the basis for studies devoted to precipitation kinetics<sup>18,19</sup> or surface and interface phase stability<sup>20–22</sup> for example.

Semi-empirical atomic interaction potentials were also employed to study the Co-Pt system. Due to the great interest associated with the use of nanoalloys with the L1<sub>0</sub> structure in high density recording media, the CoPt composition was intensively investigated. In most parametrizations of the tight-binding formalism within the second moment approximation of the electronic density (TB-SMA), the ordering temperature is below the measured one (within a 15%-50% interval)<sup>23–26</sup>. A recent calibration provides better results since the ordering temperature of the CoPt and CoPt<sub>3</sub> phases were in good agreement with experiments<sup>22</sup>. However, the asymmetry of the phase diagram with respect to the equiatomic composition was not reproduced. Indeed, the transition temperature of the Co<sub>3</sub>Pt phase is also close to  $T = 1000$  K instead of  $T = 830$  K. The Embedded Atom Model (EAM) was not more successful<sup>27</sup>. Encouraging results have been provided by a Modified EAM (MEAM) model, which successfully reproduces the asymmetry between the L1<sub>2</sub> structures with deviations of 7-8% from experimental values<sup>28</sup>. The ordering temperature of the L1<sub>0</sub> phase is however 12% lower than in measurements and 100 K lower than the one related to the CoPt<sub>3</sub> phase.

With the objectives of (i) determining if the strong concentration dependence of  $\tilde{V}_1$  is related to the sample magnetic state at the measured temperatures, (ii) acquiring quantitative data on the SRO developing at temperatures close to the ordering temperature, (iii) providing interaction energy for developing reliable atomic potentials, we have carried out neutron diffuse scattering measurements on CoPt single crystals. EPI are deduced within the ICVM. Monte Carlo simulations are performed to calculate transition temperatures, SRO, LRO, and phase equilibria related to the measured and reported EPI for the Co-Pt system.

## II. NEUTRON DIFFUSE SCATTERING MEASUREMENTS

### A. Experimental details

A CoPt single crystal of equiatomic composition was grown using the Bridgman technique from a polycrystalline ingot prepared by arc melting of 4N metals under an argon atmosphere. The crystal bar was homogenized with a 168 hours heat treatment at 1373 K under secondary vacuum ended by air quench. Three cuboidal specimen with dimensions close to  $4.5 \text{ mm} \times 4.5 \text{ mm} \times 4.5 \text{ mm}$  and faces oriented parallel to a (001) (for two of them) and 110-type (for the other four) crystallographic planes were then shaped with the spark erosion technique.

To minimize absorption and multiple scattering effects, the three samples were stacked up for the neutron measurements. After the first measurements at  $T_{\text{ds}} = 1203 \text{ K}$  and  $T_{\text{ds}} = 1423 \text{ K}$  with horizontal (001) faces ((001) diffraction plane), each sample was rotated by 90 degrees to switch to the (110) diffraction plane.

Diffuse scattering measurements were performed with the D7 time-of-flight spectrometer of the Institut Laue-Langevin (ILL) using an unpolarized neutron flux with an incident wavelength of  $\lambda = 3.02 \text{ \AA}$ . The 4-slits chopper rotation frequency was 133 Hz. The samples were wrapped in a niobium foil fixed on a high temperature boron nitride holder in a high temperature furnace mounted on a  $\omega$ -rotation stage (the furnace rotation axis is vertical). The scattered intensity was recorded with four banks of 16  $^3\text{He}$ -gas detectors covering the diffraction angles,  $2\theta$ , from  $-80^\circ$  to  $145^\circ$  with a step of about  $3^\circ$ . The  $\omega$  sample rotation extended on  $180^\circ$  with a  $2^\circ$  step at  $T_{\text{ds}} = 1203 \text{ K}$  and a  $4^\circ$  step at  $T_{\text{ds}} = 1423 \text{ K}$ . The incident beam was monitored from its diffusion by a niobium foil. Signals with the empty furnace and with an absorber (a Gd rod with the same width and place as the sample) were registered at the two temperatures in order to correct the signal from instrumental background. Measurements with a vanadium rod was also made in the same geometries at room temperature to calibrate the detectors.

A time-of-flight (TOF) analysis was performed to separate the elastic signal from the phonon and magnetic inelastic contributions, which are quite important at the investigated temperatures. The elastic intensity was modeled by a trapezoid convoluted by a Gaussian shape adjusted on the signal measured on the vanadium reference sample at  $T = 300 \text{ K}$

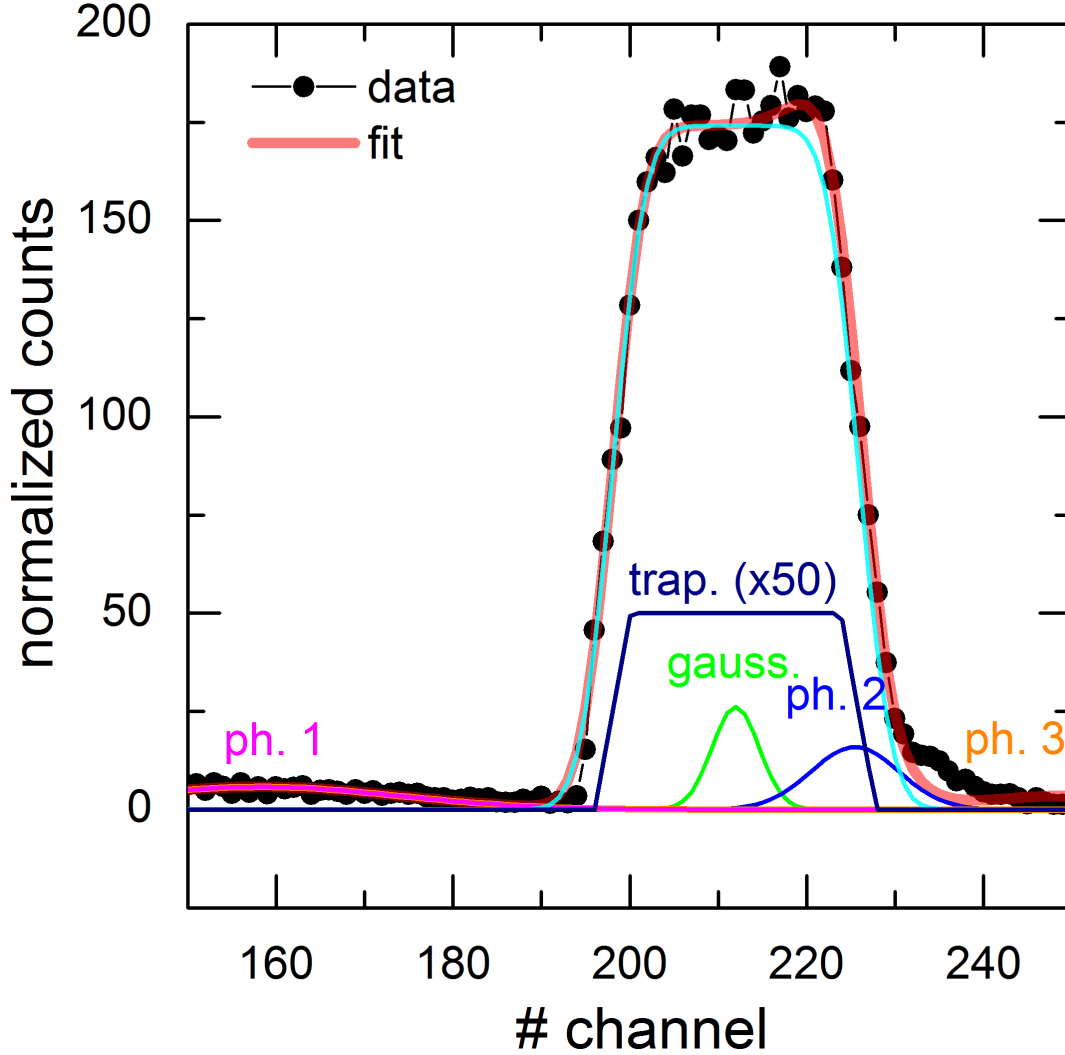


FIG. 1. (Color online) Typical neutron time-of-flight spectrum recorded at  $T_{\text{ds}} = 1423$  K in the CoPt sample. Circles correspond to experimental data and lines to the separation of elastic and inelastic contributions: in cyan: elastic contribution = a trapeze (in dark blue) convoluted by a gaussian (in green); in blue: quasi-elastic phonon; in orange (respectively magenta): high- (respectively low-) energy phonon; in red: sum of all contributions. The channel width is  $7.32 \mu\text{s}$  and the elastic line-width is close to  $2.2(9)$  meV.

(Fig. 1). The elastic line-width was close to 2.2 meV. Inelastic and quasi-elastic scattering (phonons) were modeled by Gaussian functions. For further analysis, we only considered spectra where elastic and inelastic contributions were well-separated. Moreover, spectra where a high elastic signal was originating from the high temperature chamber (detected

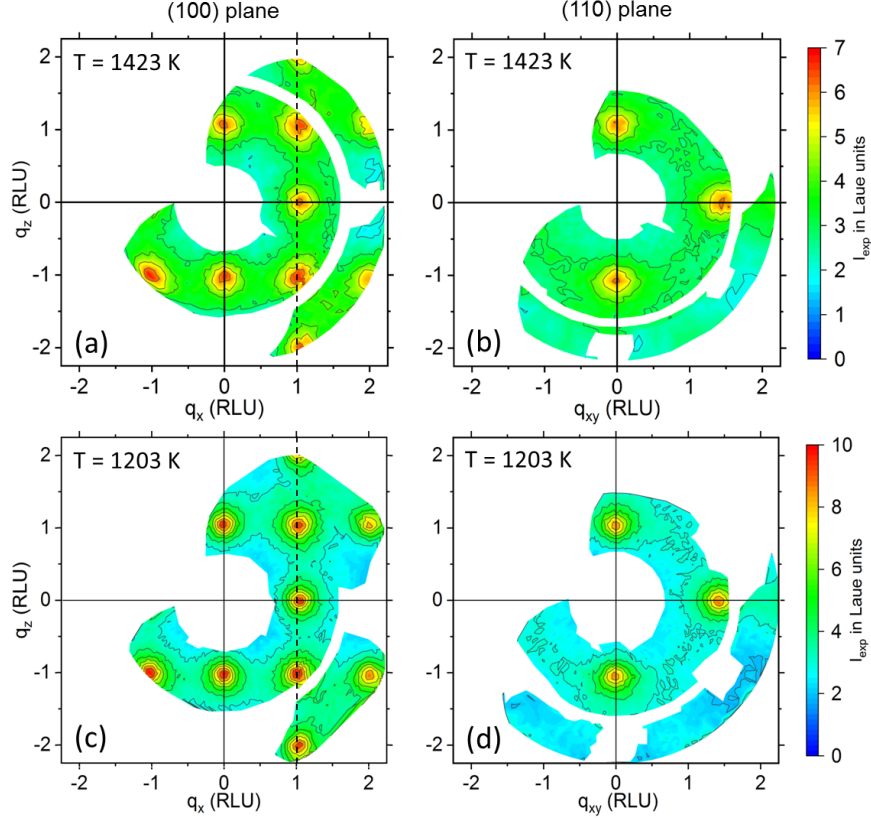


FIG. 2. Corrected intensity in CoPt at  $T_{\text{ds}} = 1423$  K : (a) (001) and (b) (110) diffraction planes and at  $T_{\text{ds}} = 1203$  K : (c) (001) and (d) (110) diffraction planes.  $q_{xy}$  is the vector along the  $[1\bar{1}0]$  direction in reciprocal lattice units (RLU). The dashed line in (a) indicates the location of the intensity profile shown in Fig. 4.

in the empty furnace signal) or from the sample Bragg peaks were also discarded. Diffuse scattering maps used to calculate the short-range order parameters finally consisted of more than 2200 relevant data points in each diffraction plane for measurements at  $T_{\text{ds}} = 1203$  K and more than 1300 points in each plane at  $T_{\text{ds}} = 1423$  K. The maps are plotted in reciprocal lattice units ( $1 \text{ RLU} = 2\pi/a \text{ \AA}^{-1}$ ) using the lattice parameter  $a$  measured by Leroux *et al.*<sup>1</sup>.

The intensities deduced from the TOF spectra were corrected for instrumental background, detector efficiency, dynamic atomic displacements (Debye-Waller attenuation), multiple scattering and sample absorption with the procedures reported by Kentzinger *et al.*<sup>16</sup>. The corrected intensity is referred to as  $I_{\text{exp}}$ . In the following, intensities are expressed in Laue units (LU), which is defined by:  $1 \text{ LU} = Nx(1-x)(b_{\text{Co}} - b_{\text{Pt}})^2$ , with  $b_{\text{Co}} = 2.49 \pm 0.02$

fm and  $b_{\text{Pt}} = 9.60 \pm 0.01$  fm, the Co and Pt nuclear coherent scattering lengths,  $N$  the number of atoms in the sample and  $x$  the concentration of Pt. In a fully disordered alloy,  $I_{\text{exp}}$  is constant and equal to 1 LU.

## B. Experimental results

The intensity maps measured at  $T_{\text{ds}} = 1423$  K and  $T_{\text{ds}} = 1203$  K for the (001) and (110) reciprocal lattice planes are shown in Fig. 2. The white areas correspond to domains where no measurement could be done or to excluded regions where a precise determination of the diffuse intensity was not possible due to the sample or the furnace Bragg peaks, or due to too large inelastic contributions.

Some diffuse intensity maxima are clearly observed around the superstructure positions – (100) and equivalents – revealing a strong short-range order.  $I_{\text{exp}}$  is modulated at  $T_{\text{ds}} = 1203$  K (respectively  $T_{\text{ds}} = 1423$  K) between  $2.1 \pm 0.4$  LU (respectively  $1.85 \pm 0.35$  LU) for the lowest values and  $10.2 \pm 1.1$  LU (respectively  $6.7 \pm 0.7$  LU) for the highest values. The relative error bars are 9% at the superstructure peaks and below 20% in the lowest-intensity ranges. As expected the diffuse intensity decreases with increasing temperature. The maps show the symmetries expected in a cubic lattice in the two investigated planes. The displacements are small because, in the intensity maps, there is neither a significant shift of the maxima positions from the superstructure positions, nor an asymmetry of the peaks, nor a detectable difference between (100)-, (110)-, and (120)-type superstructure peaks.

## III. DATA ANALYSIS

### A. Short-range-order parameters

The corrected intensities were then used to determine the Warren-Cowley short-range order parameters defined as:

$$\alpha_{\mathbf{p}} = \alpha_p = 1 - P^{A(B)}(\mathbf{r}_{\mathbf{p}})/c_A, \quad (1)$$

where  $P^{A(B)}(\mathbf{r}_{\mathbf{p}})$  is the probability to have an A atom on the site  $\mathbf{r}_{\mathbf{p}} = \frac{a}{2}(l, m, n)$ , knowing that there is a B atom at the origin.  $\mathbf{p}$  stands for the integers  $(l, m, n)$  and  $p$  for the number of the shell occupied by site  $(lmn)$  and its equivalents by symmetry. A positive (respectively

negative)  $\alpha_p$  value corresponds to an attractive (respectively repulsive) chemical interaction between the central atom and the atoms of the same species in the  $p$ -th shell.

The separation of the contributions related to the chemical SRO and the static atomic displacements was achieved using the Borie and Sparks<sup>29</sup> formulation. The method, adapted when small displacements occur, consists in writing the modulated intensity as a sum of a term associated with the correlations between chemical species and terms related to static displacements. In  $\text{CoPt}_3$ <sup>16</sup> and  $\text{Co}_{3-\epsilon}\text{Pt}_{1+\epsilon}$  alloys<sup>5</sup>, the first order term in the displacement expansion was sufficient to have a good description of the scattered intensity in spite of a 13% atomic size mismatch between cobalt and platinum. Local distortions may be indeed small even for large atomic size differences. In this study, the measured intensities were thus also described using the first order development in the displacements  $\mathbf{u}_p$  at lattice site  $\mathbf{r}_p$ :

$$I_{\text{exp}}(\mathbf{q}) = I_{\text{SRO}}(\mathbf{q}) + I_{\text{D1}}(\mathbf{q}) + I_{\text{cst}}, \quad (2)$$

where  $\mathbf{q}$  is the scattering vector,  $I_{\text{cst}}$  is a constant term related to incoherent scattering, whereas  $I_{\text{SRO}}$  and  $I_{\text{D1}}$  are the short-range order and displacement contributions, cross sections per atom in Laue units given by:

$$I_{\text{SRO}}(\mathbf{q}) = \sum_{\mathbf{p}>0} \alpha_p \cos(\mathbf{q} \cdot \mathbf{r}_p) = \alpha(\mathbf{q}) \quad (3)$$

$$I_{\text{D1}}(\mathbf{q}) = \sum_{i=1}^3 h_i Q_i(\mathbf{q}), \quad (4)$$

where  $\{h_i\}$  are the coordinates of the scattering vector in  $2\pi/a$  units (RLU). The quantities  $Q_i(\mathbf{q})$  are related to the Fourier transform of the first-order displacement parameters  $\gamma_p^i$ :

$$Q_i(\mathbf{q}) = \sum_{\mathbf{p}} \gamma_p^i \sin(\mathbf{q} \cdot \mathbf{r}_p) \quad (5)$$

In an equiatomic alloy, the displacement parameters  $\gamma_p^i$  are defined by :

$$\gamma_p^i = -\frac{2\pi}{a} \sum_{\tau, \tau'} \frac{b_\tau b_{\tau'}}{\Delta b^2} \rho_{2,p}(\tau\tau') \langle \Delta \mathbf{u}_{p,i}^{\tau\tau'} \rangle, \quad (6)$$

where  $\langle \Delta \mathbf{u}_{p,i}^{\tau\tau'} \rangle$  is the average relative displacement between atoms of type  $\tau$  and  $\tau'$  (*i.e.* Co and Pt) separated by  $r_p$ .  $\rho_{2,p}(\tau\tau')$  is the probability of finding atoms  $\tau$  and  $\tau'$  at a distance  $r_p$ . It is equal to  $(1 + \alpha_p)/4$  and  $(1 - \alpha_p)/4$  for homochemical (CoCo or PtPt) and heterochemical (CoPt) pairs, respectively.  $\Delta b$  is the usual contrast factor:  $\Delta b = b_{\text{Co}} - b_{\text{Pt}}$ .

In Eq. 2, the  $q$ -independent term has the following form :

$$I_{\text{cst}} = 1 + I_{\text{nucl}} + I_{\text{para}}, \quad (7)$$

where the first term on the right-hand side, unity, is the SRO contribution when  $\mathbf{r}_p = \mathbf{0}$ , the second term is the incoherent nuclear scattering arising from isotopic and nuclear spin disorder and the last term is related to the incoherent cross section due to magnetic moments of electrons in the paramagnetic phase. The last two contributions are calculated respectively with incoherent nuclear scattering cross sections and magnetic moments reported for Co and Pt atoms. For the sake of readability, the calculations are detailed in Appendix B.  $I_{\text{cst}}$  is found equal to  $3.14 \pm 0.33$  LU assuming that Co atoms hold their room temperature moments and  $2.55 \pm 0.14$  LU assuming that they have zero magnetic moments. The Pt moment is assumed to disappear in the paramagnetic phase.

A least-squares procedure was used to reproduce the corrected data with Eq. 2 using sets of SRO parameters  $\alpha_p$  and first order displacement parameters  $\gamma_p^i$ . After an analysis of the sensitivity to the number of p shells in Eqs. 3 and 4, the best results were obtained with  $N_{\text{SRO}} = 20$  and  $N_{\text{D1}} = 7$  for both temperatures investigated. The corresponding values are reported in Appendix A (Tab. II and Tab. III).  $I_{\text{cst}}$  was  $2.992 \pm 0.010$  LU at  $T_{\text{ds}} = 1203$  K and  $2.962 \pm 0.015$  at  $T_{\text{ds}} = 1423$  K. The paramagnetic moments thus do not change significantly between the two temperatures and are equal to  $1.52 \pm 0.06 \mu_B$  on average. The paramagnetic state so pertains to a situation where Co atoms hold their room temperature moments (within experimental uncertainties<sup>30</sup>).

The contributions to the diffuse intensity calculated with the obtained SRO and first order displacement parameters are represented in Fig. 3 for measurements at  $T_{\text{ds}} = 1423$  K and  $T_{\text{ds}} = 1203$  K.  $I_{\text{SRO}}$  presents all symmetries of a cubic reciprocal space (mirrors, rotation and translation symmetries);  $I_{\text{D1}}$  presents the mirrors including O, the origin in the reciprocal space, and  $\pi/4$  (only in (001) plane) and  $\pi/2$  rotations around O due to the  $h_i$  term in Eq. (4). Only the top-right quarters of the simulated maps are shown as they can be extended taking into account the symmetry planes including O. Note that the scales are different for  $I_{\text{D1}}$  that is much smaller in amplitude than  $I_{\text{SRO}}$  and presents changes of sign. The  $\gamma_p^i$  values are lower than 0.07, which is consistent with the hypothesis of small displacements amplitudes assumed in the Borie and Spark formalism<sup>29</sup>. They are also of the same order of magnitude as those measured for a CoPt<sub>3</sub> alloy<sup>16</sup>.

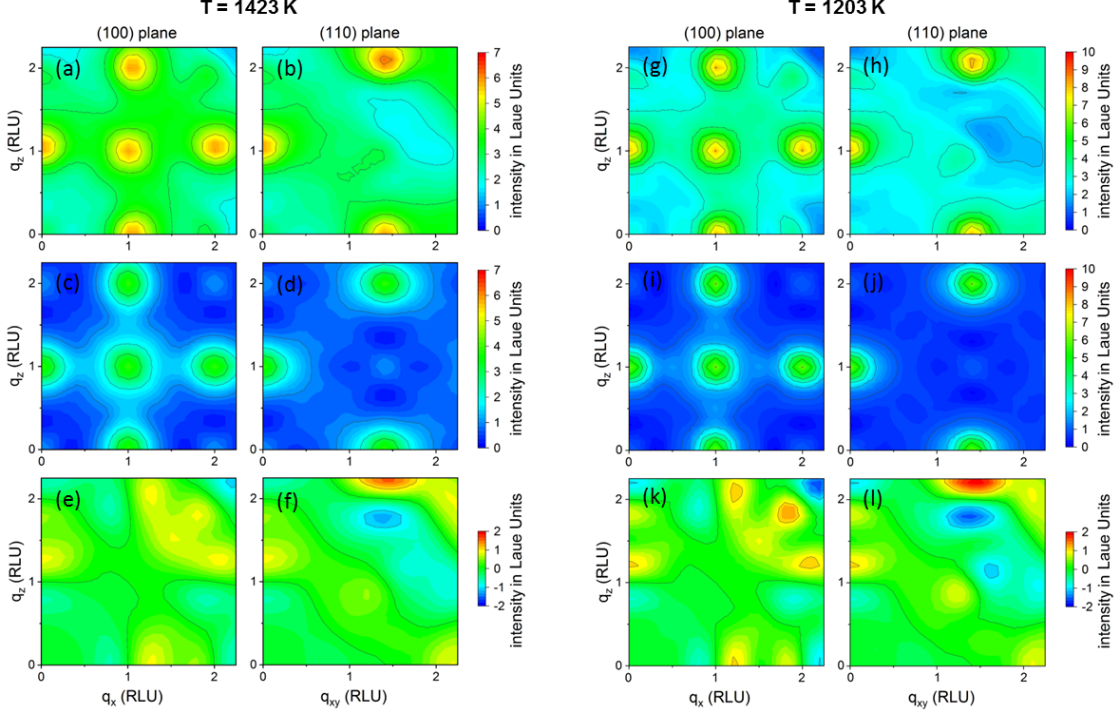


FIG. 3. Simulated intensities in the (001) and (110) planes in CoPt at  $T_{ds} = 1423$  K and  $T_{ds} = 1203$  K : (a)-(b), (g)-(h) total intensity, (c)-(d), (i)-(j) short-range order contribution ( $I_{SRO}$ ), and (e)-(f), (k)-(l) first order displacement contribution ( $I_{D1}$ ). Note that the intensity scales differ between (a) to (d) and (e) or (f) as well as between (g) to (j) and (k) or (l).

The agreement between experimental and simulated intensities is assessed by analyzing profiles going through four superstructure reflections, which are associated with SRO parameters of the alloy (dashed lines in Fig. 2). The intensity profiles related to measurements at  $T_{ds} = 1423$  K and at  $T_{ds} = 1203$  K are represented in Fig. 4. Experimental data correspond to symbols with error bars and calculations to colored lines whose thickness indicates the uncertainty resulting from the data processing. For  $T_{ds} = 1423$  K, the intensity at the maxima is satisfyingly reproduced with  $N_{SRO} = 20$  (Fig. 4a). For  $T_{ds} = 1203$  K, increasing  $N_{SRO}$  from 20 to 30 allows to increase the intensity at the maxima and to reach the experimental error bars, but it strongly increases the uncertainty on the resulting values (Fig. 4b). In addition, the first SRO parameters are not sensitive to the variation of  $N_{SRO}$ . Therefore, twenty parameters were used to describe the short-range order in the CoPt alloy. Since measurements were performed about 100 K above the ordering temperature, the difficulty

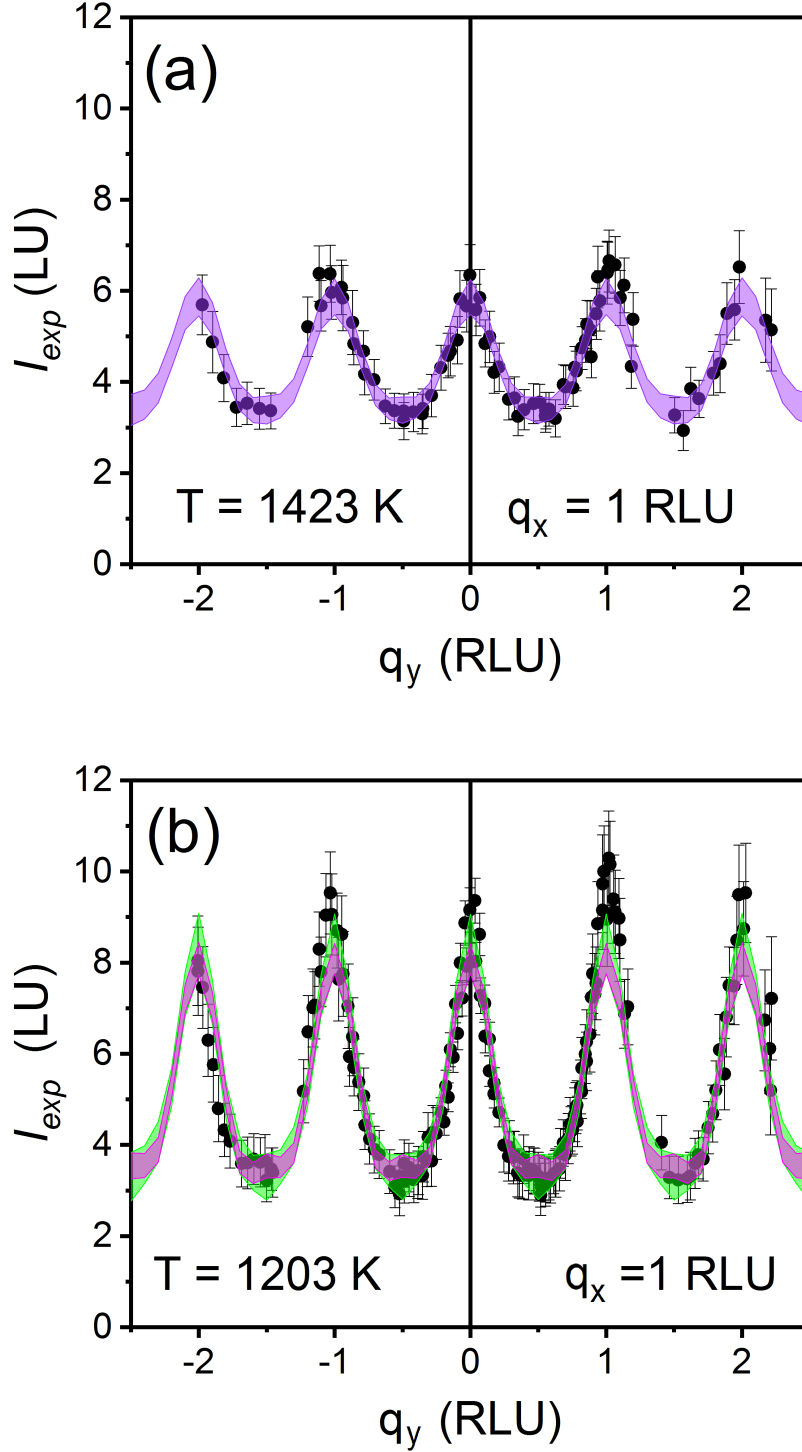


FIG. 4. Experimental (black bullets) and simulated intensities (taking into account the cumulated error bars by an area) along the  $q_x = 1$  RLU line in CoPt (a) at  $T_{\text{ds}} = 1423$  K (violet area:  $N_{\text{SRO}} = 20$ ).  $N_{\text{D1}} = 7$  and (b) at  $T_{\text{ds}} = 1203$  K (violet area:  $N_{\text{SRO}} = 20$  and green area :  $N_{\text{SRO}} = 30$ )

TABLE I. EPI ( $\tilde{V}_i$ ) obtained from neutron diffuse scattering measurements at  $T_{ds} = 1423$  K and  $T_{ds} = 1203$  K in the  $\text{Co}_{0.5}\text{Pt}_{0.5}$  alloy using ICVM. Order-disorder temperatures ( $T_{OD}$ ) are calculated using Monte Carlo simulations. Results arising from EPI reported in the literature are also listed in the last two columns.

	ICVM	ICVM	CE	TBIM
	1423 K	1203 K	[12]	[22]
$\tilde{V}_1$ (meV)	$14.88 \pm 1.00$	$12.56 \pm 0.67$	10.35	34.5
$\tilde{V}_2$ (meV)	$-4.85 \pm 0.65$	$-7.32 \pm 0.47$	-4.75	8
$\tilde{V}_3$ (meV)	$0.07 \pm 0.48$	$0.78 \pm 0.39$	4.35	8
$\tilde{V}_4$ (meV)	$-3.00 \pm 0.35$	$-1.26 \pm 0.16$	2.8	0
$\tilde{V}_6$ (meV)	$-0.05 \pm 0.24$	$-0.22 \pm 0.14$	0	0
	ordering temperature ( $T_{OD}$ )			
$T_{\tilde{V}_1-\tilde{V}_4}$ (K)	$1085 \pm 87$	$1005 \pm 48$	480	1120
$T_{\tilde{V}_1-\tilde{V}_6}$ (K) <sup>a</sup>	$1095 \pm 95$	$1025 \pm 65$	480	1120

<sup>a</sup> with  $\tilde{V}_5 = 0$

to fully match measurements with simulations for  $T_{ds} = 1203$  K is probably inherent to some pre-transitional effects.

## B. EPI from inverse cluster variation method

The next step was to determine the effective pair interactions (EPI) from the experimental values of SRO parameters  $\alpha(r_p)$ . This was performed with the ICVM previously used to fit SRO data for  $\text{CoPt}_3$  in [16] and for  $\text{Fe}_{0.804}\text{V}_{0.196}$  in [31]. The Hamiltonian of the system was described by:

$$H(\{p_i\}) = \frac{1}{2} \sum_{i,j \neq i=1}^N \tilde{V}(r_{ij}) \sigma_i \sigma_j, \quad (8)$$

with  $\tilde{V} = (V_{\text{CoCo}} + V_{\text{PtPt}} - 2V_{\text{CoPt}})/4$ , the EPI which depend on the distance  $r_{ij} = r_p$  between atoms located in a fixed FCC lattice.  $\sigma_i = \pm 1$ , is the spin variable related to the occupation of the atomic site  $i$ . In the C-O approximation, the farthest pairs considered are the sixth neighbor pairs. Nevertheless, the fifth neighbor pairs are excluded since they do not belong to the maximum clusters, the face-centered cube and the 13-point cubo-octahedron<sup>32</sup>. However, it can be assumed that they have a weak contribution to the alloy stability since the amplitude of SRO parameters decrease in the following order: second, first, fourth, sixth, fifth, and third (Tab. II in Appendix A). The EPI obtained from our measurements are listed in the upper part of Tab. I (ICVM) as well as those reported in the literature<sup>12,22</sup> and based on rigid FCC lattice calculations. The values determined from the neutron diffuse scattering measurements significantly differ from those obtained from the cluster expansion approach (CE) and the tight-binding Ising model (TBIM). The repercussions on transition temperatures and short-range order are discussed in Sec. IV.

### C. Monte Carlo calculations (MC)

With the aim of determining the order-disorder (OD) temperatures and the SRO parameters, the EPI obtained from the ICVM and those reported in the literature were used as input parameters of Monte Carlo simulations carried out on a rigid FCC lattice with periodic boundary conditions. The calculations were carried out with  $20 \times 20 \times 20$  unit cells of 4 atoms. The initial configuration of the Markov chain consisted in a random solid solution. The thermodynamics of the binary alloy was described with the Hamiltonian of Eq. 8. A detailed description of the code and the methodologies developed to determine phase diagrams of binary alloys in different thermodynamic ensembles were provided in previous papers<sup>4,33</sup>.

To calculate the alloy phase diagram, the Monte Carlo simulations were performed in the semi-grand canonical  $(N, \Delta\mu, V, T)$  ensemble where the total number of atoms  $N$ , the alloy chemical potential  $\Delta\mu$ , the volume of the simulation  $V$  and the temperature  $T$  are fixed quantities. The Metropolis algorithm<sup>34</sup> is applied to changes of atomic species on single sites (Co  $\leftrightarrow$  Pt flipping mechanism). The composition was thus not conserved during

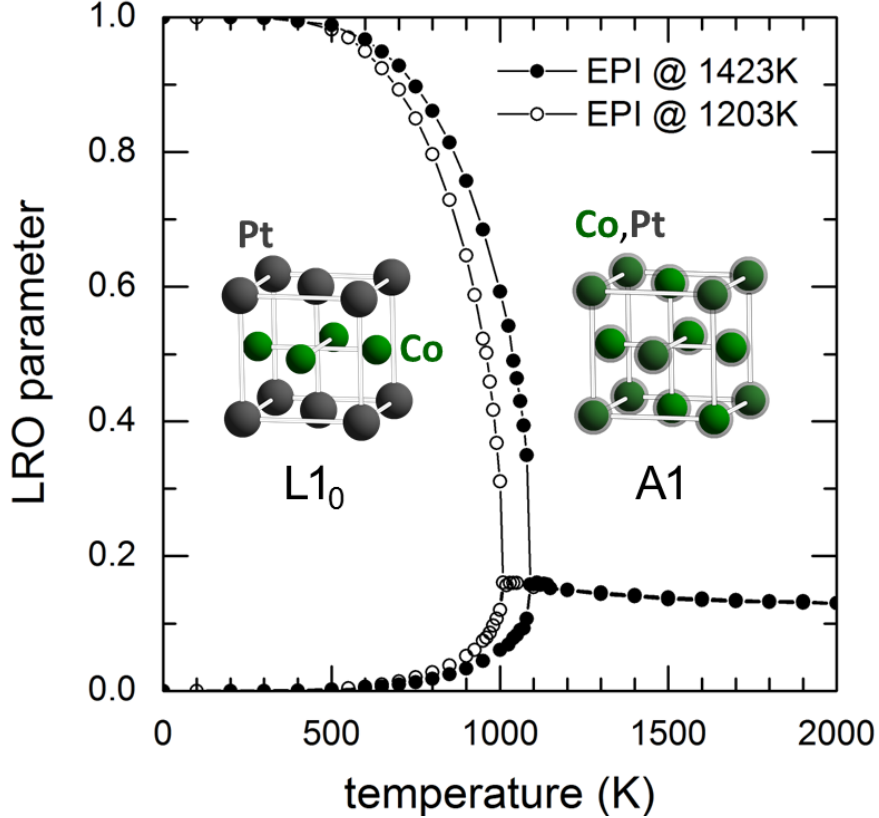


FIG. 5. Temperature dependence (5 K step size) of the CoPt alloy long-range order (LRO) parameter calculated near the transition for the two EPI sets determined in this study (see Tab. I).  $L1_0$  and A1 are respectively the ordered and the disordered structures.

the Markov chain. The advantage of the semi-grand canonical thermodynamic ensemble is that only single phases take place in the simulation, thus avoiding artificial effects caused by interfaces between ordered and disordered phases. The ordering state of the alloy is monitored as a function of the composition and the temperature with a LRO parameter defined within the concentration wave representation<sup>2,35</sup>. The order-disorder temperatures corresponding to all the EPI sets are reported in Tab. I ( $T_{OD}$ ). The temperature dependence of the LRO parameter calculated for the EPI determined at  $T_{ds} = 1203$  K and at  $T_{ds} = 1423$  K exhibits a similar behavior (Fig. 5): the two curves are superimposed in the disorder state and the discontinuity of the order parameter at the transition is the signature of a first order transformation. The amplitude of the discontinuity is 0.23 for the highest temperature and 0.16 for the lowest. This hierarchy tends to consolidate the fact that the transition is weakened by some pre-transitional effects. The transition temperature

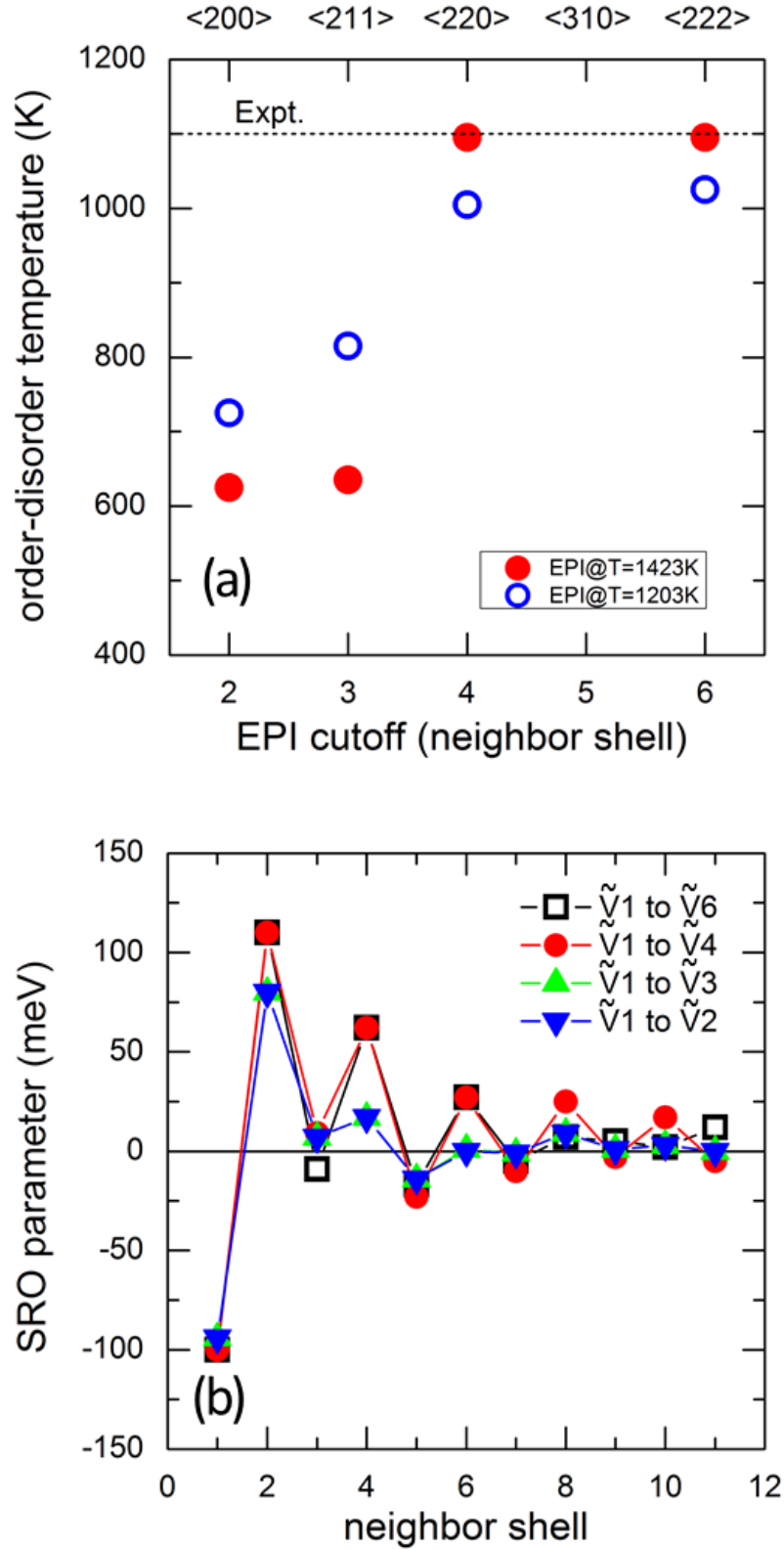


FIG. 6. (a) CoPt order-disorder temperature as a function of the EPI cutoff distance. Distances are given as neighbor shell numbers ( $p$ ) and interatomic distance coordinates ( $\mathbf{r}_p$ ) in  $a/2$  unit (bottom and top axes, respectively). The experimental transition temperature of the alloy is indicated by the dashed line. (b) SRO parameters as a function of the distance for four EPI cutoff distances.

depends on the interaction cutoff distance (Fig. 6). For EPI determined at  $T_{\text{ds}} = 1423$  K (filled symbols), a 500 K jump is indeed observed when interactions farther than the third neighbors are considered. Weak effects are observed between the second and the third, or between the fourth and the sixth interaction distances. For the EPI determined at  $T_{\text{ds}} = 1203$  K (open symbols), the transition temperature increases with the interaction distance up to the fourth neighbor shell and then stabilizes at temperatures close to 1000 K. Monte Carlo calculations thus show that interactions up to the fourth neighbor atomic shell are required to reproduce the experimental order-disorder transition temperature. The effects of the accuracy of EPI on the transition temperature have been assessed with Monte Carlo simulations. The ordering temperature variations are close to  $\pm 90$  K and  $\pm 60$  K for the two sets of EPI (see Tab. I), which is consistent with the used formalism<sup>16</sup>.

To calculate SRO parameters, the Monte Carlo simulations were performed in the canonical  $(N_{\text{Co}}, N_{\text{Pt}}, V, T)$  ensemble where the number of cobalt  $N_{\text{Co}}$  and platinum  $N_{\text{Pt}}$  atoms, the volume of the simulation  $V$  and the temperature  $T$  are fixed quantities. The Metropolis algorithm<sup>34</sup> is applied to exchanges between particles to reproduce chemical correlations (Co  $\leftrightarrow$  Pt swapping mechanism). The composition is thus conserved. The initial configuration is equilibrated by  $5 \times 10^5$  swapping attempts per atomic site before computing the Warren-Cowley parameters with the following equation:

$$\alpha_p = \frac{\bar{\rho}_p - y^2}{1 - y^2}, \quad (9)$$

with  $y = 2N_{\text{Pt}}/N - 1$  and  $\bar{\rho}_p$ , the configurational average of the spin variable product  $\sigma_n \sigma_m$  where the atomic site  $m$  is located in the  $p$ -th neighbor shell of the atomic site  $n$ . The values of  $\alpha_p$  are calculated every 100 Monte Carlo step (MCS), where a MCS consists in  $N$  swapping attempts. The mean value and the standard deviation were finally determined from 1000 values of  $\alpha_p$ . The results related to the different EPI sets are represented up to the eleventh atomic shell in Fig. 7(b) and the numerical values are listed in Appendix C (Tab. I) for the sake of readability. This analysis of these results is provided in the following section.

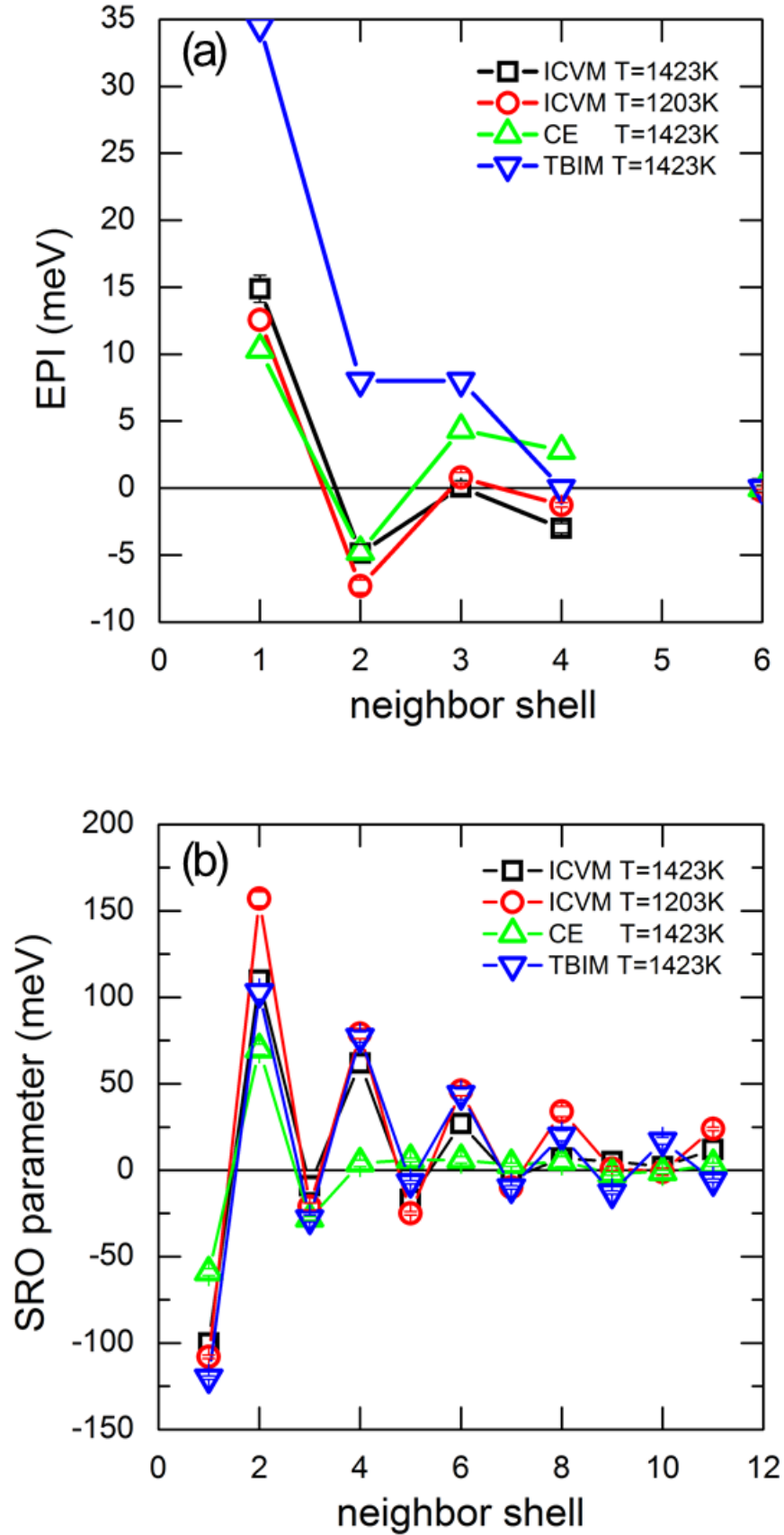


FIG. 7. (a) Effective pair interactions and related (b) SRO parameters as a function of  $p$ , the atomic neighbor shell number, in the CoPt alloy.

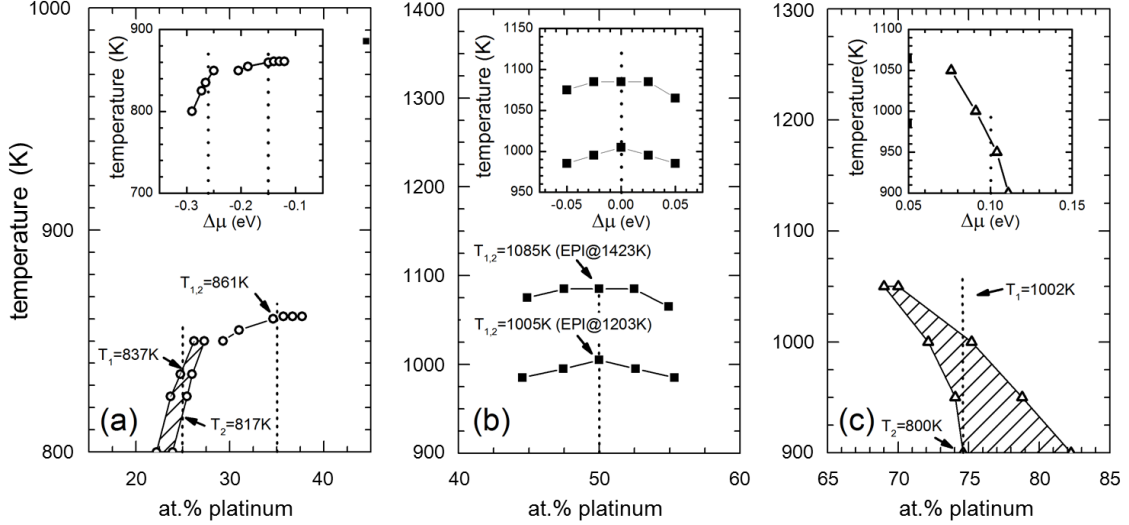


FIG. 8. Composition-temperature phase diagrams calculated using Monte Carlo simulations in the semi-grand canonical thermodynamic ensemble close to  $\text{Co}_{0.75}\text{Pt}_{0.25}$  (a),  $\text{Co}_{0.5}\text{Pt}_{0.5}$  (b), and  $\text{Co}_{0.75}\text{Pt}_{0.25}$  (c). The corresponding chemical potential-temperature ( $\Delta\mu$ - $T$ ) phase diagrams are represented in the insets.  $T_1$  and  $T_2$  are the upper and lower limits of the two-phase (ordered-A1) range deduced from experimental EPI at the measurement concentrations. It is referred to as  $T_{1,2}$  when these two temperatures are not distinguishable.

#### IV. DISCUSSION

Neutron diffuse scattering measurements were carried out at two temperatures close to the order-disorder transition of the CoPt alloy. The main outcome is the determination of the effective pair interactions (EPI) which reproduce (i) the short-range order developing close to the transition as well as (ii) the experimental ordering temperature,  $T_{\text{OD}}$ . The temperature sensitivity of the EPI allowed to evaluate (i) the reliability of the results, and (ii) the presence of magnetic or pre-transitional effects. The analysis of the constant term of the diffuse scattering cross section resulted in the estimate of the average magnetic moment in the paramagnetic regime. Using Monte Carlo simulations, the phase stability of the alloy at and around to the equiatomic composition and the uncertainties related to the data analysis were investigated. The importance of interactions up to the fourth atomic neighbor shell was pointed out. In order to evaluate the stability of these approaches to predict accurately the SRO state and the order-disorder temperature at the CoPt composition,

the EPI obtained at high temperature were confronted to those arising from theoretical studies based on the cluster expansion (CE) and the tight-binding Ising model (TBIM). By considering all the diffuse scattering measurements carried out for the Co-Pt system<sup>5,16</sup>, we obtain the concentration dependence of the EPI providing the basis for the development of reliable atomic interaction potentials that can reproduce the composition-temperature phase diagram of the Co-Pt alloy (such EPI were still missing at present). We now discuss all these aspects based on the results presented above.

Temperature effects. The neutron diffuse scattering measurements were carried out at temperatures 383 K and 603 K higher than the Curie temperature of the alloy ( $T_{CM} = 820$  K in the disordered A1-CoPt<sup>6</sup>). In this high temperature range, magnetic correlations were expected to be negligible and the EPI should correspond to the mean field limit, thus being temperature independent<sup>36</sup>. This is verified in this study; differences were not more than a few meV between the two measurement temperatures (Fig. 7a). Such variations were of the order of the usual accuracy provided by the measurement technique and by the hypotheses made in the data analysis<sup>16</sup>. The temperature dependence of the EPI mainly affected the SRO parameters related to the shells farther than the fourth atomic neighbor distance with relative deviations in the 22%-44% interval (Fig. 7b). Moreover, the deduced ordering temperature ( $T_{OD}$ , see Tab. I) is close to the experimental one (1098 K). A 10% difference (100 K) was observed between the two measurement temperatures. Since the accuracy of the ordering temperature determination is close to 90 K, it is not possible to affirm that this difference is inherent to some physical effects.

The  $q$ -independent term of the diffuse scattering intensity differed by about 1% between the two investigated temperatures. Therefore, the average paramagnetic moment of  $1.52 \pm 0.06 \mu_B$ , determined from the measurements, was not significantly modified by temperature.

Importance of interactions. Starting from the EPI determined up to the sixth neighbor shell, the influence of the interaction distance on the ordering temperature and the short-range order close to the transition was investigated with Monte Carlo simulations. Considering the interaction between sixth neighbors (sites at the ends of the body diagonal of the cubic unit cell) increases the ordering temperature by 53% in comparison to the situation where interactions up to the second or up to the third neighbors are considered (Fig. 6a). A good agreement with the experimental temperature was obtained only in calculations which

use interactions farther than the third neighbor shell. The discontinuity of the LRO parameter at the transition temperature followed the behavior found at the ordering temperature: a value of  $0.43 \pm 0.01$  was calculated when interactions up to the third neighbor shell were considered and a value of  $0.23 \pm 0.01$  was calculated when considering interactions up to the fourth and sixth atomic distances. The SRO parameters calculated with interactions up to the second and third neighbor shells were similar due to the weak value of  $\tilde{V}_3$  and strongly differed from the SRO parameters calculated with interaction up to the sixth neighbor shell in terms of amplitude and sign (Fig. 6b). When EPI related to the fourth neighbor shell were included, the SRO parameters of the two sets were equal for distances up to the eighth neighbors. Farther, SRO parameters related to interactions up to the fourth neighbor shell exhibited non zero values (Fig. 6b).

Reliability of the reported EPI. The EPI measured in this study can be compared to those reported in the literature for the CoPt alloy. Fig. 7(a) represents the EPI calculated by Chepulskii *et al.*<sup>12</sup> using the cluster expansion approach (CE) and those deduced by Lopes *et al.*<sup>22</sup> within a tight-binding Ising model (TBIM). The corresponding ordering temperature and SRO parameters are provided in Tab. I and in Fig. 7(b) respectively. EPI obtained from the CE were rather close to those measured in this study. However, the SRO parameters and the ordering temperature (450 K) were not in good agreement with experimental results. This shows that some missing contributions play a significant role in the thermodynamics of CoPt alloys (e.g., vibrational free energy<sup>14</sup>, electronic excitations<sup>15</sup>). EPI obtained from TBIM are strongly different from the EPI derived in this study but the SRO parameters are in good qualitative agreement. For the first neighbor shells, relative errors are indeed in the 10%-25% interval depending on the temperature. 41% and 102% discrepancies are, however, observed for  $\alpha_2$  at 1203 K and  $\alpha_3$  at 1423 K. As expected, the ordering temperature is equal to the measured. Indeed, this was a constrain in the determination of EPI<sup>22</sup>. The relatively good description by the TBIM EPI of SRO developing close to the ordering temperature has to be pointed out because the transition temperature is the only information directly related to the high temperature thermodynamics which was included in the fitting procedure.

Concentration dependence of EPI and magnetism. Diffuse scattering measurements had previously been performed for  $\text{Co}_{0.75}\text{Pt}_{0.25}$ ,  $\text{Co}_{0.65}\text{Pt}_{0.35}$  and  $\text{Co}_{0.25}\text{Pt}_{0.75}$  compositions<sup>5,16</sup>. The EPI are summarized in Appendix C (Tab. V) and the phase diagram calculated with Monte Carlo simulations at and around each composition is represented in Fig. 8. Around

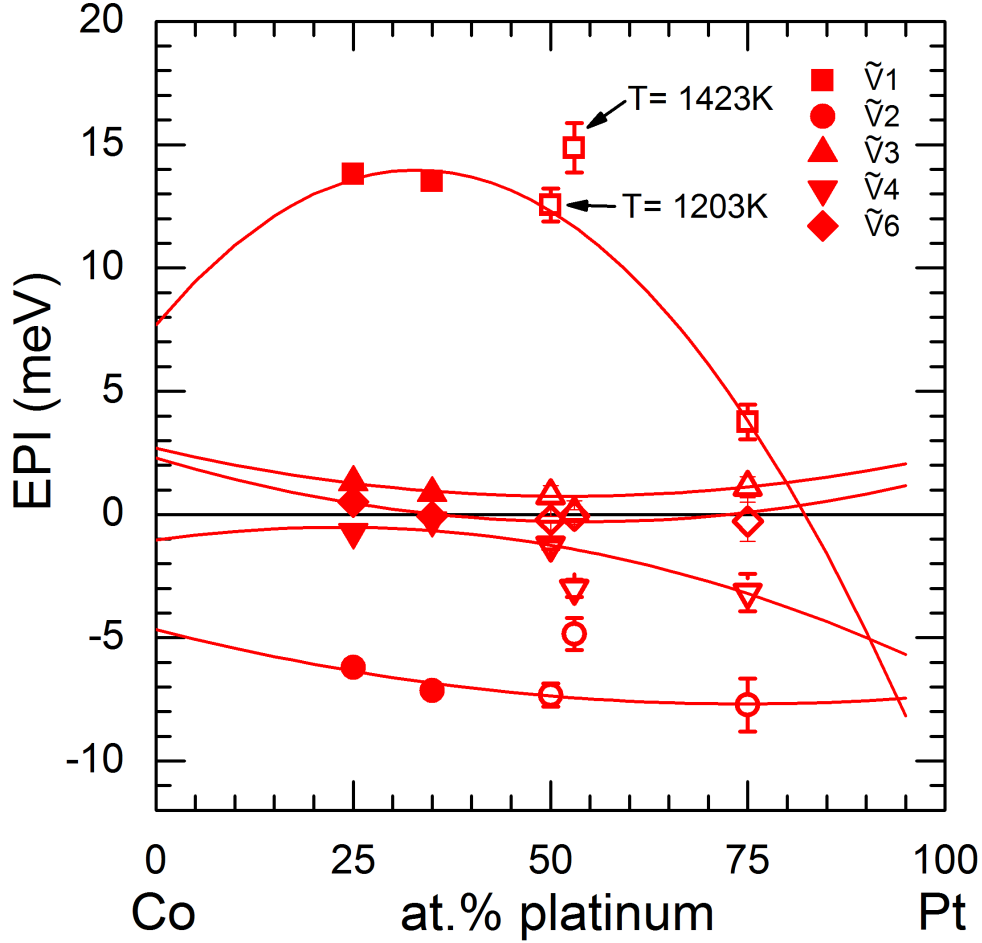


FIG. 9. Composition dependence of effective pair interactions (EPI) determined from diffuse scattering and ICVM in the Co-Pt system. Red lines are guidelines (parabolic fits). Data corresponding to  $T_{ds} = 1423\text{K}$  are displaced by  $\Delta c = 0.03$  for the sake of clarity. Filled symbols correspond to measurements in the ferromagnetic state, open symbols to measurements in the paramagnetic state.

the  $\text{Co}_{0.75}\text{Pt}_{0.25}$  alloy, the diagram features a narrow two-phase domain (Fig. 8(a)) with an ordering temperature close the temperatures determined experimentally by Inden<sup>37</sup> and Capitan *et al.*<sup>5</sup> ( $\approx 830\text{K}$ ). The ordering related to the  $\text{Co}_{0.25}\text{Pt}_{0.75}$  alloy was also shown to correspond to a two-phase domain with a transition temperature close the one determined experimentally (Fig. 8(c))<sup>16</sup>. The composition dependence of the EPI determined from all the diffuse scattering measurements in the Co-Pt system is represented in Fig. 9 with open (respectively full) symbols for ferro- (respectively para-) magnetic state of the alloy at the temperatures of the diffuse scattering measurements. The data sets from this study are

those at  $x = 0.5$ . For the sake of readability, the EPI measured at  $T_{\text{ds}} = 1423$  K are shifted in composition by  $\Delta c = 0.03$ . Red lines are quadratic fits to the EPI measured in the previous studies<sup>5,16</sup>. For the CoPt alloy, the EPI measured at  $T_{\text{ds}} = 1203$  K follow quite well the fits. The calculated ordering temperature is, however, 75 K below the experimental one. The EPI measured at 1423 K deviate by a few meV from the quadratic behavior. The transition temperature is nevertheless equal to the experimental one. This is consistent with the formation enthalpy of the  $L1_0$  structure, which writes:

$$\Delta E_{L1_0} = -16\tilde{V}_1 - 32\tilde{V}_3 - 32\tilde{V}_5, \quad (10)$$

for interactions up to the sixth atomic shell. Assuming that  $\tilde{V}_5$  is zero,  $\Delta E_{L1_0}$  is  $-226 \pm 23$  meV. $\text{atom}^{-1}$  for  $T_{\text{ds}} = 1203$  K and  $-240 \pm 31$  meV. $\text{atom}^{-1}$  for  $T_{\text{ds}} = 1423$  K.

In Fig. 9, the EPI determined in the paramagnetic state for the  $\text{Co}_{0.5}\text{Pt}_{0.5}$  alloy do not exhibit a singular behavior with respect to those determined in the ferromagnetic state for the compositions  $\text{Co}_{0.75}\text{Pt}_{0.25}$  and  $\text{Co}_{0.65}\text{Pt}_{0.35}$ . The drop in the composition dependence of  $\tilde{V}_1$  is therefore not caused by the change of the magnetic state at the measurement temperature.

At high temperatures, in the chemically disordered state ( $A1$  structure), the average magnetic moment of the CoPt alloy was estimated to be  $1.52 \pm 0.06 \mu_B$  and temperature independent. This value is close to the magnetic moment of ferromagnetic cobalt ( $1.76 \pm 0.26 \mu_B$ ) obtained from X-ray magnetic circular dichroism (XMCD) measurements at room temperature and *ab initio* calculations<sup>30</sup>. It is also in agreement with the Curie-Weiss-type behavior observed in the ordered and disordered states<sup>38</sup>, as expected from the fact that pure cobalt is a strong ferromagnet. The magnetic moment of cobalt is therefore only weakly modified by temperature ( $0 \text{ K} < T < 1423 \text{ K}$ ), by the magnetic state (ferromagnetic/paramagnetic), and by the chemical order ( $L1_0/A1$ ). This induces that the concentration dependence of the measured EPI is not related to some magnetic moment variations.

Phase diagram. Phase stabilities in the Co-Pt system have been experimentally investigated by various techniques: X-ray diffraction, electronic microscopy, and electrical resistivity measurements<sup>1,37,39</sup>. The resulting phase diagram is represented in Fig. 10 by black lines and dots. The Co-rich domain has not been studied extensively because of the slow atomic diffusion at temperatures close to  $T_{\text{OD}}$ , the transition temperature. For cross-checking purposes, three samples with the  $\text{Co}_{0.75}\text{Pt}_{0.25}$  composition were sealed in quartz tubes, one in each, homogenized for 48 h at 1273 K and then annealed at 823 K, 830 K, and 843 K for

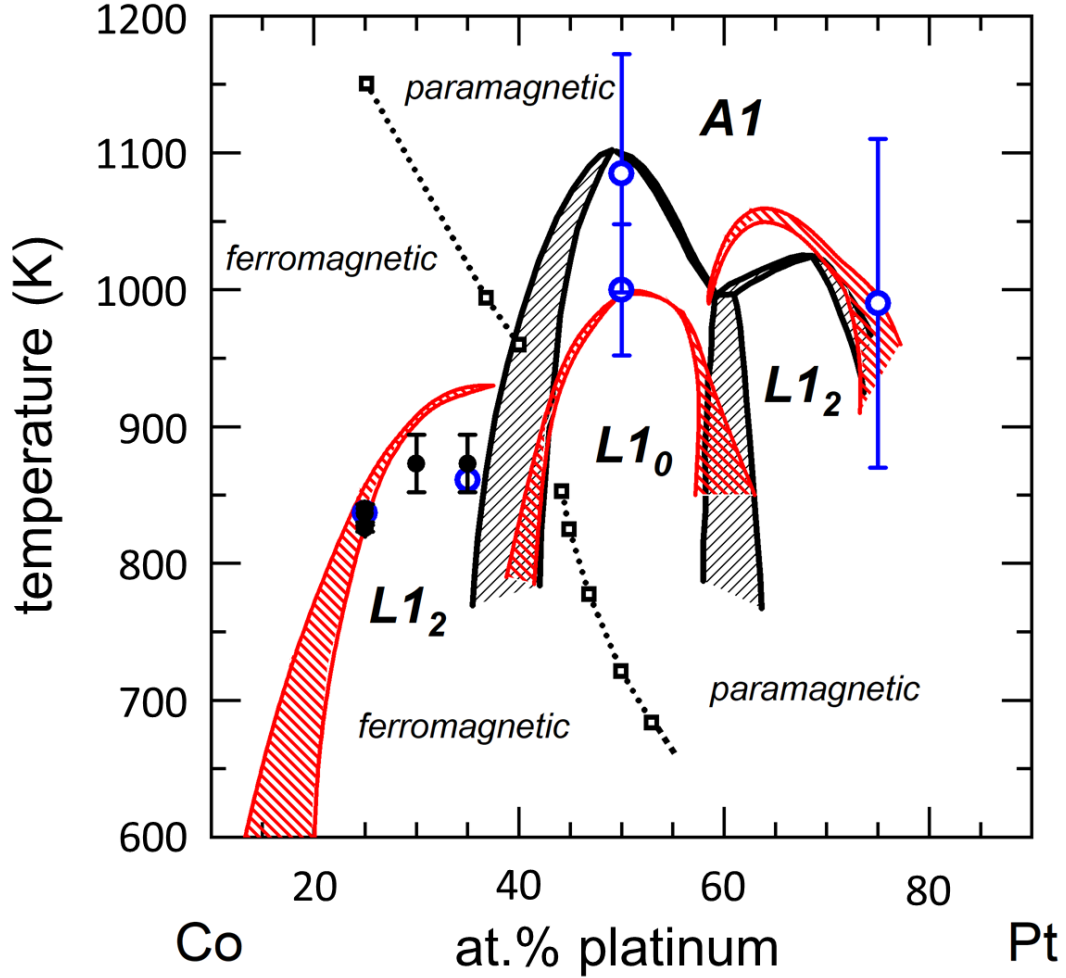


FIG. 10. Experimental phase diagram of the Co-Pt system from the work of Inden *et al.*<sup>37</sup>, Leroux *et al.*<sup>1</sup> and Le Bouar *et al.*<sup>39</sup>, in black. Blue open circles are the phase boundaries derived from Monte Carlo calculations using the EPI determined from diffuse scattering experiments<sup>5,16,40</sup> (symbols in Fig. 9). Red hatched regions are ordered/disordered two-phase domains calculated using a quadratic composition dependence of EPI (line in Fig. 9)

74, 62, and 62 days, respectively. The order-disorder transition temperature determined by transmission electron microscope observations was estimated in the 830 K-843 K range, in agreement with the reported values by Inden *et al.*<sup>37</sup> and Capitan *et al.*<sup>5</sup> (Appendix D).

The order-disorder transition temperatures calculated from the data provided by all the diffuse scattering measurements are also superimposed in Fig. 10 (blue circles). The errors bars, close to 125 K, have been estimated from the uncertainties related to the EPI determi-

nation<sup>16</sup>. A good agreement between experimental and calculated ordering temperatures is obtained, notwithstanding the accuracy of the EPI determination and the simplicity of the model. Magnetic, elastic effects as well as electronic entropy are indeed neglected in such a rigid lattice approach.

For the sake of comparison, the phase diagram calculated with the quadratic composition dependence of EPI (Fig. 9) is superimposed (red lines) to the experimental phase diagram. This approximation leads to a qualitative description of the phase stability only. The ordering temperatures, asymmetry of the phase diagram, compositions related to congruent transformations are not fully reproduced.

## V. CONCLUSION

The phase stability of the CoPt alloy was investigated close to its order-disorder transition temperature ( $T_{OD} = 1100$  K) using neutron diffuse scattering experiments. The effective pair interactions (EPI) obtained from measurements carried out at 1423 K and 1203 K indicate that, provided the accuracy of the technique and the hypotheses made in the data analysis, the EPI belong to the mean field limit, thus being temperature independent. Temperature mainly affects atomic shells farther than the fourth neighbor distance yielding a 100 K variation of the calculated order-disorder transition temperature. The comparison of EPI with those reported in the literature within the cluster expansion<sup>12</sup> and the tight binding Ising model<sup>22</sup> shows that the TBIM EPI provide a relatively good description of the alloy thermodynamics at temperatures close to ordering temperature (short-range order and temperature of phase transformation), even if they strongly differ from the EPI determined in this study.

The determined EPI complete those already measured for the  $\text{Co}_{0.75}\text{Pt}_{0.25}$ , the  $\text{Co}_{0.65}\text{Pt}_{0.35}$ , and the  $\text{Co}_{0.25}\text{Pt}_{0.75}$  compositions.<sup>5,16</sup> Their composition dependence shows that the EPI determined in the paramagnetic state for the  $\text{Co}_{0.5}\text{Pt}_{0.5}$  alloy do not significantly differ from those determined in the ferromagnetic state for  $\text{Co}_{0.75}\text{Pt}_{0.25}$  and  $\text{Co}_{0.65}\text{Pt}_{0.35}$ . The drop in the composition dependence of EPI related to the first neighbor atomic shell is therefore not caused by the change of the magnetic state at the measurement temperature.

Transmission electron microscope observations carried out on several annealed  $\text{Co}_{0.75}\text{Pt}_{0.25}$  samples confirmed that the order-disorder transition takes place in the 830 K-843 K tem-

perature interval. The synthesis of the experimental and numerical studies devoted to the Co-Pt phase stability show that the simulation of its phase diagram is not yet satisfactory. Improvements would imply to incorporate both magnetic and elastic effects, which are usually neglected in rigid lattice approaches<sup>8</sup>.

## ACKNOWLEDGMENTS

The authors acknowledge A. Finel for helpful discussions on neutron diffuse scattering analysis with the ICVM approach and the French-German ANR-DFG MAGIKID project for some support.

### Appendix A: SRO and first order displacements parameters obtained from the data processing

The measured intensities are described using the first order development in the atomic displacements (Eqs. 2-4). A least-squares procedure was used to reproduce the corrected data using sets of SRO parameters  $\alpha_p$  and first order displacement parameters  $\gamma_p^i$ . The best results were obtained with  $N_{\text{SRO}} = 20$  and  $N_{\text{D1}} = 7$  for both of the investigated temperatures. The corresponding values of  $\alpha_p$  and  $\gamma_p^i$  are given in Tab. II and Tab. III, respectively, for the two measurement temperatures.

### Appendix B: Derivation of the q-independent contribution in neutron diffuse scattering

The incoherent cross sections found in the tables correspond to the contributions due to isotopic distribution and to nuclear moments:  $\sigma_{inc}^{tab}(\text{Co}) = 4.8 \pm 0.3$  barn and  $\sigma_{inc}^{tab}(\text{Pt}) = 0.13 \pm 0.11$  barn. Using a rule of mixtures, we get  $\sigma_{inc}^{tab}(\text{CoPt}) = 2.465 \pm 0.205$  barn and  $I_{inc}^{tab}(\text{CoPt}) = 1.55 \pm 0.14$  Laue units (LU).

In the paramagnetic state, a supplementary contribution has to be added: the incoherent cross section due to the average paramagnetic quadratic magnetic moments  $\overline{M_\mu^2}$  on species

TABLE II. SRO parameters ( $\alpha_p$ ) obtained from neutron diffuse scattering measurements at  $T_{ds} = 1203$  K and  $1423$  K in the  $\text{Co}_{0.5}\text{Pt}_{0.5}$  alloy.

$p$	$l$	$m$	$n$	$\alpha_p^{T_{ds}=1203K}$	$\alpha_p^{T_{ds}=1423K}$
1	1	1	0	-0.1078(21)	-0.1002(19)
2	2	0	0	0.1568(19)	0.1102(20)
3	2	1	1	-0.0230(13)	-0.0091(11)
4	2	2	0	0.0788(12)	0.0619(12)
5	3	1	0	-0.0250(10)	-0.0171(10)
6	2	2	2	0.0464(13)	0.0272(13)
7	3	2	1	-0.0099(6)	-0.0046(6)
8	4	0	0	0.0339(15)	0.0071(18)
9	3	3	0	0.0014(10)	0.0049(11)
10	4	1	1	-0.0011(7)	0.0016(8)
11	4	2	0	0.0244(8)	0.0120(9)
12	3	3	2	-0.0013(9)	0.0024(9)
13	4	2	2	0.0159(7)	0.0025(8)
14	4	3	1	-0.0051(5)	-0.0024(5)
15	5	1	0	-0.0101(9)	-0.0053(9)
16	5	2	1	-0.0050(6)	-0.0009(6)
17	4	4	0	0.0139(10)	0.0068(11)
18	4	3	3	-0.0020(9)	0.0004(8)
19	5	3	0	-0.0035(7)	-0.0006(8)
20	4	4	2	0.0094(8)	0.0041(8)

TABLE III. First order displacement parameters ( $\gamma_p^\beta$ ) obtained from neutron diffuse scattering measurements at  $T_{\text{ds}} = 1203$  K and 1423 K in the  $\text{Co}_{0.5}\text{Pt}_{0.5}$  alloy.

$p$	$\gamma_p^x$	$\gamma_p^y$	$\gamma_p^z$
$T_{\text{ds}} = 1203\text{K}$			
1	0.0624(10)	0.0624(10)	0
2	-0.0398(20)	0	0
3	-0.0090(10)	-0.0014(7)	-0.0014(7)
4	-0.0136(9)	-0.0136(9)	0
5	0.0199(9)	0.0090(9)	0
6	-0.0040(9)	-0.0040(9)	-0.0040(9)
7	0.0147(7)	0.0019(7)	0.0026(6)
$T_{\text{ds}} = 1423\text{K}$			
1	0.0670(12)	0.0670(12)	0
2	-0.0386(26)	0	0
3	-0.0095(11)	-0.0045(8)	-0.0045(8)
4	-0.0125(12)	-0.0125(12)	0
5	0.0102(10)	0.0058(11)	0
6	-0.0007(10)	-0.0007(10)	-0.0007(10)
7	0.0067(7)	0.0004(8)	0.0022(7)

$\mu$ . Assuming  $g = 2$  (neglecting the spin-orbit coupling), it can be written as<sup>41</sup>:

$$\left(\frac{d\sigma}{d\Omega}(q)\right)_{H=0}^T = \frac{2}{3} \left(\frac{\gamma e^2}{2m_e c^2}\right)^2 F(q)^2 \sum_{\mu} N_{\mu} \overline{M_{\mu}^2} \quad (\text{B1})$$

where  $N_{\mu}$  is the number of  $\mu$  atoms,  $m_e$  and  $e$  the electron mass and charge,  $c$  the speed of light and  $\gamma$  the neutron gyromagnetic ratio. We can assume that  $F(q)$ , the magnetic form factor, is constant in the investigated  $q$ -range:  $(\frac{\gamma e^2}{2m_e c^2})^2 F(q)^2 \approx 72.65 \text{ mbarn}\cdot\text{sr}^{-1}\cdot\text{atom}^{-1}$ .

The magnetic moments in CoPt have been measured using X-ray magnetic circular dichroism (XMCD) at 300 K by Grange *et al.*<sup>30</sup>:  $\mu_{\text{Co}} = 1.76 \pm 0.26 \mu_B$  and  $\mu_{\text{Pt}} = 0.35 \pm 0.05 \mu_B$  (we assume a 0.15 relative error bar, typical for XMCD). As the Pt moment is induced by a polarization of its electronic bands by the average Co moment, the Pt moments disappear at the Curie temperature. We thus obtain an upper limit for the paramagnetic incoherent contribution per atom:  $I_{\text{para}} = 0.59 \pm 0.19 \text{ LU}$ . The value of the constant term in the experimental data is finally:  $I_{\text{cst}} = 1 + I_{\text{nucl}} + I_{\text{para}} = 3.14 \pm 0.33 \text{ LU}$  assuming that Co atoms keep their 300 K moment and  $I_{\text{cst}} = 2.55 \pm 0.14 \text{ LU}$  assuming that all Co moments disappear.

### Appendix C: EPI and related SRO parameters calculated with Monte Carlo simulations

The EPI obtained from the measurements and those reported in the literature are used as input parameters of Monte Carlo simulations carried out in a rigid FCC lattice with periodic boundary conditions.

- To calculate the transition temperatures, the Monte Carlo simulations are performed in the semigrand-canonical  $(N, \Delta\mu, V, T)$  ensemble where the total number of atoms  $N$ , the alloy chemical potential  $\Delta\mu$ , the volume of the simulation  $V$  and the temperature  $T$  are fixed quantities. In this ensemble only single phases take place in the simulation. The ordering state of the alloy is monitored as a function of the composition and the temperature with a LRO parameter. The order-disorder transition temperatures corresponding to all the EPI sets analyzed in this study are listed in Tab. IV for the  $\text{Co}_{0.5}\text{Pt}_{0.5}$  alloy and in Tab. V for other compositions ( $T_{\text{OD}}$ ).

- To calculate SRO parameters, the Monte Carlo simulations are performed in the canonical  $(N_{\text{Co}}, N_{\text{Pt}}, V, T)$  ensemble where the number of cobalt and platinum atoms,  $N_{\text{Co}}$  and  $N_{\text{Pt}}$ , the volume of the simulation  $V$  and the temperature  $T$  are fixed quantities. The Warren-

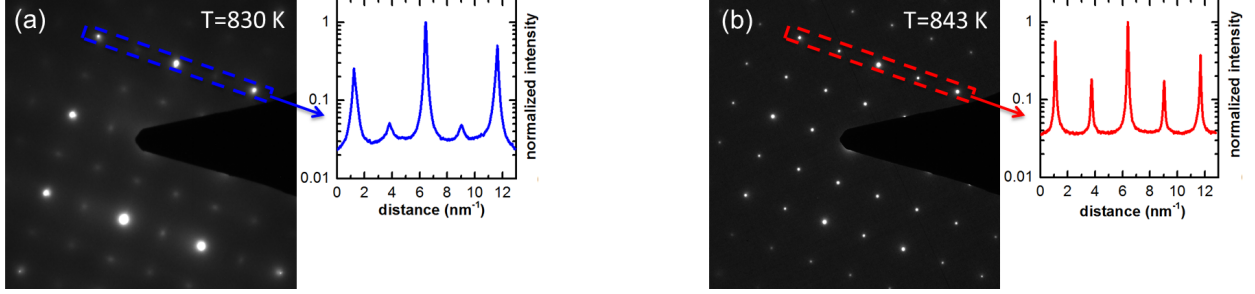


FIG. 11. TEM observations. Selected area electron diffraction (SAED) pattern recorded in the  $[001]$  zone axis of a  $\text{Co}_{0.75}\text{Pt}_{0.25}$  sample (a) at  $T = 830$  K, (b) at  $T = 843$  K. Insets: intensity profiles associated with the dashed boxes.

Cowley parameters  $\alpha_p$  are calculated with Eq. 9. The results related to the different EPI sets are listed up to the eleventh atomic shell in Tab. IV for the  $\text{Co}_{0.5}\text{Pt}_{0.5}$  alloy.

#### Appendix D: Transmission electron microscope observations of the $\text{Co}_{0.75}\text{Pt}_{0.25}$ alloy

$\text{Co}_{0.75}\text{Pt}_{0.25}$   $\phi 3 \text{ mm} \times 250 \mu\text{m}$  annealed discs were mechanically thinned to  $50 \mu\text{m}$  using 1200, 2400 and 4000 paper-grit and then diamond suspensions ( $3 \mu\text{m}$  and  $1 \mu\text{m}$ ). The specimens were then ion-polished with a GATAN Precision Ion Polishing System (PIPS) in dual beam mode. Finally, observations were carried out in a FEI CM20 transmission electron microscope operating at 200 kV. Diffraction patterns acquired along  $[001]$  zone axis in samples annealed at  $T_a = 830$  K and  $T_a = 843$  K are represented in Fig. 11. Lines profiles, represented in the insets, reveal that the intensity ratio between the superstructure peaks related to the  $L1_2$  phase and the (200) fundamental peak related to solid solution is 15% for  $T_a = 830$  K and 2% for  $T_a = 843$  K.

TABLE IV. EPI ( $\tilde{V}_i$ ) and SRO parameters ( $\alpha_p$ ) obtained from neutron diffuse scattering measurements at  $T_{\text{ds}} = 1423$  K and 1203 K in the CoPt alloy using ICVM. Order-disorder temperatures ( $T_{\text{OD}}$ ) were calculated using Monte Carlo simulations. Results arising from EPI reported in the literature are also listed in the last two columns.

	ICVM	ICVM	CE	TBIM
	1423 K	1203 K	[12]	[22]
$\tilde{V}_1$ (meV)	14.88(100)	12.56(67)	10.35	34.5
$\tilde{V}_2$ (meV)	-4.85(65)	-7.32(47)	-4.75	8
$\tilde{V}_3$ (meV)	0.07(48)	0.78(39)	4.35	8
$\tilde{V}_4$ (meV)	-3.00(35)	-1.26(16)	2.8	0
$\tilde{V}_6$ (meV)	-0.05(24)	-0.22(14)	0	0
order-disorder temperature ( $T_{\text{OD}}$ )				
$T_{\tilde{V}_1-\tilde{V}_4}$ (K)	1085(87)	1005(48)	480	1120
$T_{\tilde{V}_1-\tilde{V}_6}$ (K) <sup>a</sup>	1095(95)	1025(65)		
p	$\alpha_p$			
1	-0.100(2)	-0.108(2)	-0.059(2)	-0.120(1)
2	0.110(2)	0.157(1)	0.070(3)	0.103(4)
3	-0.009(1)	-0.023(1)	-0.028(1)	-0.028(2)
4	0.062(1)	0.079(1)	0.004(2)	0.077(3)
5	-0.017(1)	-0.025(1)	0.006(1)	-0.007(1)
6	0.027(1)	0.046(1)	0.006(2)	0.044(3)
7	-0.005(1)	-0.010(1)	0.003(1)	-0.010(1)
8	0.007(2)	0.034(2)	0.005(3)	0.020(3)
9	-0.005(1)	0.001(1)	-0.002(1)	-0.013(1)
10	0.002(1)	-0.001(1)	-0.001(1)	0.017(2)
11	-0.012(1)	<sup>32</sup> -0.024(1)	0.003(1)	-0.006(1)

TABLE V. EPI ( $\tilde{V}_i$ ) reported from diffuse scattering measurements in the Co-Pt system. Order-disorder temperatures ( $T^{MC}$ ) calculated using Monte Carlo simulations are compared to measured ones ( $T^{exp}$ ).

	Co <sub>0.75</sub> Pt <sub>0.25</sub>	Co <sub>0.65</sub> Pt <sub>0.35</sub>	Co <sub>0.25</sub> Pt <sub>0.75</sub>
	[5]	[5]	[16]
$\tilde{V}_1$ (meV)	13.81	13.52	3.76(70)
$\tilde{V}_2$ (meV)	-6.21	-7.15	-7.73(107)
$\tilde{V}_3$ (meV)	1.31	0.87	1.11(43)
$\tilde{V}_4$ (meV)	-0.73	-0.24	-3.17(76)
$\tilde{V}_6$ (meV)	0.51	0.08	-0.29(80)
	order-disorder temperature		
$T^{exp}$ (K)	830		996
$T^{MC}$ (K)	837	861	1002(104)

\* Mathieu.Fevre@onera.fr

<sup>1</sup> C. Leroux, M. C. Cadeville, V. Pierron-Bohnes, G. Inden, and F. Hinz, *J. Phys. F: Met. Phys.* **18**, 2033 (1988).

<sup>2</sup> Y. Le Bouar, *Influence des effets elastiques lors de la mise en ordre coherente dans le systeme Co-Pt : microstructures de biphasage L1<sub>0</sub> + L1<sub>2</sub>*, Ph.D. thesis, Ecole polytechnique (1998).

<sup>3</sup> P. Andreazza, V. Pierron-Bohnes, F. Tournus, C. Andreazza-Vignolle, and V. Dupuis, *Surf. Sci. Rep.* **70**, 188 (2015).

<sup>4</sup> M. Fèvre, C. Varvenne, A. Finel, and Y. Le Bouar, *Phil. Mag.* **93**, 1563 (2013).

- <sup>5</sup> M. J. Capitan, S. Lefèbvre, Y. Calvayrac, M. Bessière, and P. Cénédèse, *J. Appl. Crystallogr.* **32**, 1039 (1999).
- <sup>6</sup> J. M. Sanchez, J. L. Moran-Lopez, C. Leroux, and M. C. Cadeville, *J. Phys. C: Solid State Phys.* **21**, L1091 (1988).
- <sup>7</sup> A. Alam, B. Kraczek, and D. D. Johnson, *Phys. Rev. B* **82**, 024435 (2010).
- <sup>8</sup> S. Karoui, H. Amara, B. Legrand, and F. Ducastelle, *J. Phys. Cond. Matter* **25**, 056005 (2013).
- <sup>9</sup> A. Bieber and F. Gautier, *J. Phys. Soc. Japan* **53**, 2061 (1984).
- <sup>10</sup> F. Ducastelle, *Order and Phase Stability in Alloys*, Cohesion and structure (North-Holland, 1991).
- <sup>11</sup> N. Braidy, Y. Le Bouar, M. Fèvre, and C. Ricolleau, *Phys. Rev. B* **81**, 054202 (2010).
- <sup>12</sup> R. V. Chepulskii and W. H. Butler, *Phys. Rev. B* **86**, 155401 (2012).
- <sup>13</sup> J. Sanchez, F. Ducastelle, and D. Gratias, *Physica A: Statistical Mechanics and its Applications* **128**, 334 (1984).
- <sup>14</sup> A. van de Walle and G. Ceder, *Rev. Mod. Phys.* **74**, 11 (2002).
- <sup>15</sup> M. Barrachin, A. Finel, R. Caudron, A. Pasturel, and A. Francois, *Phys. Rev. B* **50**, 12980 (1994).
- <sup>16</sup> E. Kentzinger, V. Parasote, V. Pierron-Bohnes, J. F. Lami, M. C. Cadeville, J. M. Sanchez, R. Caudron, and B. Beuneu, *Phys. Rev. B* **61**, 14975 (2000).
- <sup>17</sup> D. Gratias and P. Cenedese, *J. Phys. Colloques* **46**, 149 (1985).
- <sup>18</sup> M. Levesque, E. Martínez, C.-C. Fu, M. Nastar, and F. Soisson, *Phys. Rev. B* **84**, 184205 (2011).
- <sup>19</sup> E. Martínez, O. Senninger, C.-C. Fu, and F. Soisson, *Phys. Rev. B* **86**, 224109 (2012).
- <sup>20</sup> J. Creuze, I. Braems, F. Berthier, C. Mottet, G. Tréglia, and B. Legrand, *Phys. Rev. B* **78**, 075413 (2008).
- <sup>21</sup> F. Lequien, J. Creuze, F. Berthier, I. Braems, and B. Legrand, *Phys. Rev. B* **78**, 075414 (2008).
- <sup>22</sup> A. Lopes, G. Tréglia, C. Mottet, and B. Legrand, *Phys. Rev. B* **91**, 035407 (2015).
- <sup>23</sup> Z.-R. Liu, H. Gao, L. Q. Chen, and K. Cho, *Phys. Rev. B* **68**, 035429 (2003).
- <sup>24</sup> M. Allalen, H. Bouzar, and T. Mehaddene, *Eur. Phys. J. B* **45**, 443 (2005).
- <sup>25</sup> G. Rossi, R. Ferrando, and C. Mottet, *Faraday Discuss.* **138**, 193 (2008).

- <sup>26</sup> A. Front, B. Legrand, G. Tréglia, and C. Mottet, *Surf. Sci.* **679**, 128 (2019).
- <sup>27</sup> P. Moskovkin and M. Hou, *J. Alloys Compd.* **434-435**, 550 (2007).
- <sup>28</sup> S. I. Park, B.-J. Lee, and H. M. Lee, *Scripta Mater.* **45**, 495 (2001).
- <sup>29</sup> B. Borie and C. J. Sparks, Jr, *Acta Crystallogr. A* **27**, 198 (1971).
- <sup>30</sup> W. Grange, I. Galanakis, M. Alouani, M. Maret, J.-P. Kappler, and A. Rogalev, *Phys. Rev. B* **62**, 1157 (2000).
- <sup>31</sup> V. Pierron-Bohnes, E. Kentzinger, M. C. Cadeville, J. M. Sanchez, R. Caudron, F. Solal, and R. Kozubski, *Phys. Rev. B* **51**, 5760 (1995).
- <sup>32</sup> A. Finel, *Statics and Dynamics of Alloy Phase Transformations* (P.E.A. Turchi and A. Gonis, Vol. 319 of NATO Advanced Study Institute, Series B: Physics Plenum, New York, 1994) p. 495.
- <sup>33</sup> M. Fèvre, Y. Le Bouar, and A. Finel, *Phys. Rev. B* **97**, 195404 (2018).
- <sup>34</sup> N. Metropolis, A. W. Rosenbluth, M. N. Rosenbluth, A. H. Teller, and E. Teller, *J. Chem. Phys.* **21**, 1087 (1953).
- <sup>35</sup> A. Khachaturyan, *Theory of Structural Transformations in Solids* (Wiley, New York, 1983).
- <sup>36</sup> V. Pierron-Bohnes, M. C. Cadeville, A. Finel, and O. Schaerpf, *J. Phys. I France* **1**, 247 (1991).
- <sup>37</sup> G. Inden, in *Mater. Res. Soc. Symp. Proc.*, Vol. 19, edited by L. Bennett, T. Massalski, and B. Giessen (North-Holland, New York, 1983) pp. 175 – 188.
- <sup>38</sup> J. M. Sanchez, J. L. Moran-Lopez, C. Leroux, and M. C. Cadeville, *J. Phys.-Condens. Mat.* **1**, 491 (1989).
- <sup>39</sup> Y. Le Bouar, A. Loiseau, and A. Finel, *Phys. Rev. B* **68**, 224203 (2003).
- <sup>40</sup> This work.
- <sup>41</sup> W. Marshall and S. W. Lovesey, *Theory of thermal neutron scattering* (Oxford Clarendon Press, 1971)
- .